Electronic Supplementary Material (ESI) for Journal of Materials Chemistry C.
This journal is © The Royal Society of Chemistry 2021

Supporting Information

Modulation of OLED Efficiency via a Combination of Aromatic Electrophilic Directing and Intramolecular Charge Transfer

Xiancheng Nie, Tao Wang*, Wenhuan Huang, Hao Su, Biao Chen, Xuepeng Zhang* and Guoqing Zhang*

Hefei National Laboratory for Physical Sciences at the Microscale, University of Science and Technology of China, Hefei, 230026, China.

Corresponding Author

E-mail: chemwang@ustc.edu.cn;

zhangxp@ustc.edu.cn;

gzhang@ustc.edu.cn.

EXPERIMENTAL SECTION

Materials. 4-cyanobenzoyl chloride, fluorobenzene, (4-fluorophenyl)(phenyl)methanone, 3-bromo-9H-carbazole, (4-(diphenylamino)phenyl)boronic acid, aluminum trichloride and potassium tert-butoxide were purchased from Energy Chemical Co.,Ltd., Tetrakis(triphenylphosphine) palladium ($Pd(PPh_3)_4$) was acquired from Sigma-Aldrich LLC. All other reagents and solvents were acquired from Sinopharm Chemical Reagent Co., Ltd and used as received. Water was deionized with a Milli-Q SP reagent water system (Millipore) to a specific resistivity of 18.2 MΩ. cm. Analytical thin layer chromatography (TLC) was performed using glass plates pre-coated with silica gel and zinc phosphate (0.25 mm). TLC plates were visualized by exposure to UV light (UV) at 254 nm. Flash column chromatography was performed using silica gel 60 (230-400 mesh, Merck) with the indicated solvents.

Methods. ^{1}H NMR (400 MHz) spectra were collected on Bruker AV400 NMR spectrometer and operated in the Fourier transform mode at 298 K. The related chemical shifts were reported as values in ppm relative to tetramethylsilane (TMS, δ= 0) in deuterated solvents. High-resolution mass spectra (HRMS) were conducted on an Atouflex speed mass spectrometer using the electrospray ionization (ESI) mode. Gel filtration chromatography was performed using a ZORBAX SB-C18 column (Agilent) conjugated to an Agilent 1260 Infinite HPLC system. Prior to the characterization, each sample was purified via 0.22 μm filter to remove any aggregates. The flow rate was fixed at a rate of 1.5 mL/min, the injection volume was 20 μL and each sample was run for 80 min. The absorption wavelength used was set at 346 nm. Acetonitrile and water were used as the eluting solvent. Electrochemical analysis was carried out by a CHI660E instrument in a conventional three-electrode configuration system: glassy carbon electrode as working electrode, Ag/AgCl electrode as reference electrode and Pt wire electrode as counter electrode. The oxidative scans were performed using 0.1 M Bu_4NPF_6

in dichloromethane (DCM) as the supporting electrolyte and a scan rate of 100 mV s^{-1} at room temperature. Reductive scans were performed using 0.1 M Bu_4NPF_6 in dimethylformamide (DMF) as the supporting electrolyte and a scan rate of 100 mV s–1 at room temperature. The ferrocenium/ferrocene couple (Fc^+/Fc) was used as the internal reference. Thermogravimetric analysis (TGA) was performed by a METTLER TOLEDO TGA1 under nitrogen atmosphere. The temperature was increased to 700℃ with a heating rate of 10℃ min^{-1}. Differential scanning calorimetry (DSC) measurements were performed by a METTLER TOLEDO DSC1 under nitrogen atmosphere. The temperature was increased and decreased with a heating or cooling rate of 10℃ min^{-1}. The measurements were repeated 2 times and 2^{nd} cycle was utilized to determine the glass transition temperature. Single-crystal data were collected from a XtaLAB AFC12 (RINC): Kappa single diffractometer. The crystal was kept at 293 K during data collection. Using Olex2, the structure was solved with the ShelXT structure solution program using intrinsic phasing and refined with the ShelXL refinement package using least-squares minimization.UV-vis spectra were measured in various solvents on Agilent Cary 60 UV-vis spectrometer ranging from 190-1100 nm and data processed on Origin 2020. Steady-state and Time-resolved photoluminescence emission spectra were conducted on a FluoroMax-4 spectrofluorometer (Horiba Scientific) and analyzed by Origin 2020 software. Absolute quantum yields were determined using an integrating sphere. Emission lifetime decay profiles were collected on Horiba Ultima time-resolved fluorescence spectrometer with 1MHz lasers, and the related data were analyzed with DataStation v6.6 (Horiba Scientific).

Theoretical Calculations. The ground-state (S_0) geometries for all the molecules studied in this work were optimized at the functional PBE1PBE/6-31G (d, p) with Gaussian 16 package. For the sake of consistency, the singlet excited states(S_1) were calculated using time-

dependent density functional theory (TD-DFT) at the same level. Triplet states (T_1) of all molecules were assessed by spin-relaxed open-shell optimization at the PBE1PBE/6-31G (d, p) level, and then time-dependent density functional theory (TD-DFT, PBE1PBE/6-31G (d, p) was applied in order to get more detailed knowledge of TADF process. The numerical calculations were conducted on the supercomputing system in the Supercomputing Center of University of Science and Technology of China.

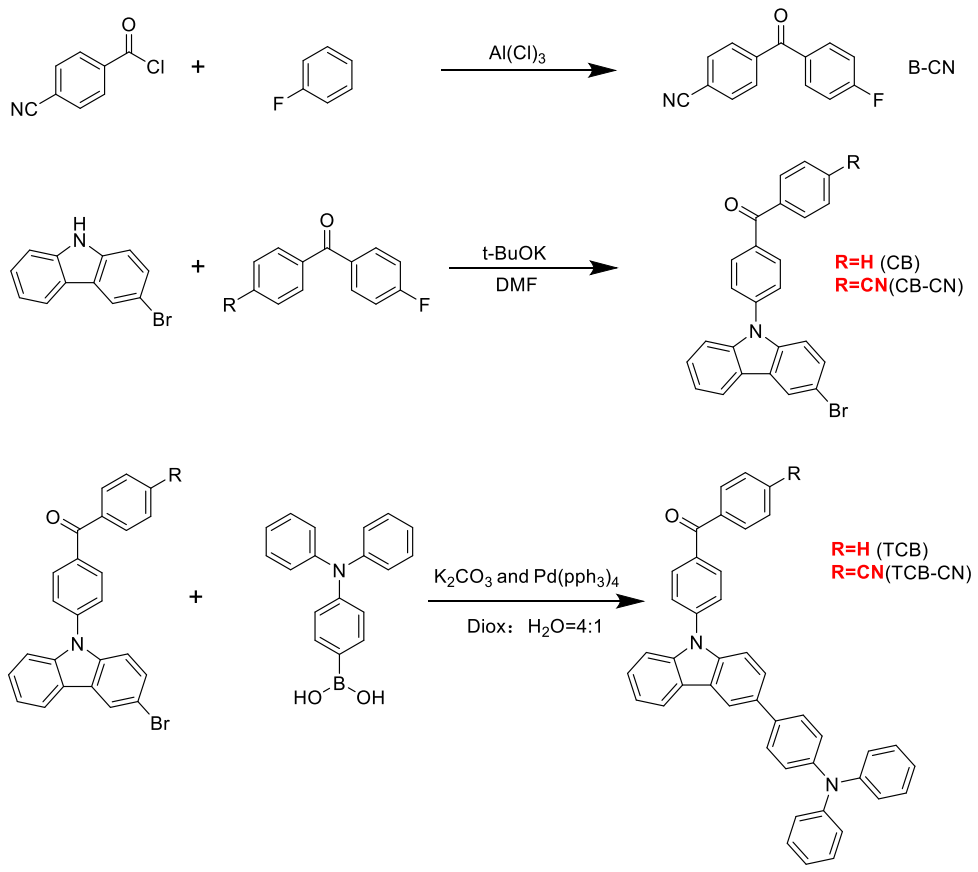

Scheme S1 Synthetic routes and chemical structures of molecules.

Synthesis of 4-(4-fluorobenzoyl)benzonitrile (**B-CN**). To a cooled (ice bath) mixture of 4-cyanobenzoyl chloride (1.5 g, 1 eq.) and fluorobenzene (8.7 g, 10 eq.) was added $AlCl_3$ (1.1 g, 1.3 eq.) in batches over a period of 15 minutes with stirring under nitrogen atmosphere. The resulting mixture was warmed to room temperature and allowed to react for 15 minutes. Then the reaction mixture was heated to reflux for 5 hours. After the reaction finished, the mixture was poured slowly into 20% aqueous HCl (30 mL) and stirred for 15 minutes. The organic layer was extracted with CH_2Cl_2 three times (40 mL ∗3) and the solvent was removed under vacuum. The crude product was further purified by column chromatography, giving a brown solid (1.54g, 76%). ^{1}H NMR (400 MHz, DMSO-d6), δ (TMS, ppm): 8.06- 8.03 (2H), 7.88- 7.84 (4H), 7.44-7.40 (2H). $[M+H]^+$ calcd for $C_{14}H_8FNO$, 226.2304; found 226.0667.

Synthesis of (4-(3-bromo-9H-carbazol-9-yl)phenyl)(phenyl)methanone (**CB**). Potassium tert-butoxide (660 mg, 1.1 eq.) was added to a round-bottom flask containing 3-bromo-9H-carbazole (1.2 g, 1 eq.) and N, N'-dimethylformamide (25 mL). The reaction was allowed to continue for an hour at room temperature. Then, (4-fluorophenyl)(phenyl)methanone (1.1 g, 1.1 eq.) was added to the reaction system and the reaction was conducted at 90 °C for 12 hours. After the reaction finished, N, N'-dimethylformamide was removed under vacuum. The crude product dissolved in CH_2Cl_2 (50 mL), washed by ionized water three times (50 mL∗3). Then CH_2Cl_2 was removed in vacuum. The collected crude product was further purified by column chromatography, giving a white solid (1.27 g, 62%). ^{1}H NMR (400 MHz, DMSO-d6), δ (TMS, ppm): 8.55 (1H), 8.35-8.33 (1H), 8.05-8.03 (2H), 7.88-7.84 (4H), 7.75- 7.71 (1H), 7.64-7.49 (6H), 7.38- 7.34 (1H). $[M+H]^+$ calcd for $C_{25}H_{16}BrNO$, 427.3210; found 426.0493.

Synthesis of (4-(3-(4-(diphenylamino)phenyl)-9H-carbazol-9-yl)phenyl)(phenyl)methanone (**CB-CN**). The synthetic method is similar to **CB** by replacing (4-fluorophenyl)(phenyl)methanone as 4-(4-fluorobenzoyl)benzonitrile. The final product is the

yellow solid (65%, 1.43 g). ^{1}H NMR (400 MHz, DMSO-d_6), δ (TMS, ppm): 8.55- 8.54(1H), 8.35-8.33 (1H), 8.10-7.98 (6H), 7.88-7.86 (2H), 7.61-7.58 (1H), 7.56-7.49 (3H), 7.38-7.34 (1H).

Synthesis of (4-(3-(4-(diphenylamino)phenyl)-9H-carbazol-9-yl)phenyl)(phenyl)methanone (**TCB**). 150 mL of 1,4-dioxane and 2 mL of K_2CO_3 aqueous solution (2 mol/L) were added into a round-bottom flask and protected by N_2. Then (4-(3-bromo-9H-carbazol-9-yl)phenyl)(phenyl)methanone (1 equiv., 0.5 g), (4-(diphenylamino)phenyl)boronic acid (1.3 equiv., 0.44 g), $Pd(PPh_3)_4$ (0.03 equiv., 0.04 g) were added to the flask. Then the reaction system was heated to reflux for 24 h. After the reaction system cooled down to room temperature, the solvent was removed under reduced pressure. Then the collected solid was re-dissolved in dichloromethane (100 mL) and washed with deionized water (100 mL) twice. The organic layer was collected and removed by the rotary evaporator in vacuum. The crude product was further purified by column chromatography to afford **TCB** as the white solid (83%, 0.58 g). ^{1}H NMR (400 MHz, CD_2Cl_2), δ (TMS, ppm): 8.37 (1H), 8.19-8.22 (1H), 8.06-8.08 (2H), 7.89-7.91 (2H), 7.76-7.78 (2H), 7.69-7.71 (1H), 7.61-7.66 (4H) , 7.54-7.59 (3H), 7.45-7.49 (1H) , 7.34-7.36 (1H) , 7.27-7.32 (4H) , 7.13-7.19 (6H) , 7.02-7.06 (2H). MALDI-TOF m/z: $[M]^+$ calcd for $C_{43}H_{30}N_2O$, 590.7260; found 590.3059.

Synthesis of 4-(4-(3-(4-(diphenylamino)phenyl)-9H-carbazol-9-yl)benzoyl)benzonitrile (**TCB-CN**). The synthetic method is similar to TCB by replacing (4-(3-bromo-9H-carbazol-9-yl)phenyl)(phenyl)methanone as (4-(3-(4-(diphenylamino)phenyl)-9H-carbazol-9-yl)phenyl)(phenyl)methanone. The final product is the off-white crystal (72%, 0.49 g). ^{1}H NMR (400 MHz, CD_2Cl_2), δ (TMS, ppm): 8.36 (1H), 8.19-8.21 (1H), 8.05-8.07 (2H), 7.96-7.98 (2H), 7.85-7.87 (2H), 7.79-7.82 (2H), 7.69-7.71 (1H), 7.61-7.64 (3H), 7.57-7.59 (1H), 7.45-7.49 (1H) ,

7.33-7.37 (1H) , 7.27-7.30 (4H) , 7.13-7.18 (6H) , 7.03-7.06 (2H). MALDI-TOF m/z: $[M]^+$ calcd for $C_{44}H_{29}N_3O$, 615.7360; found 615.7350.

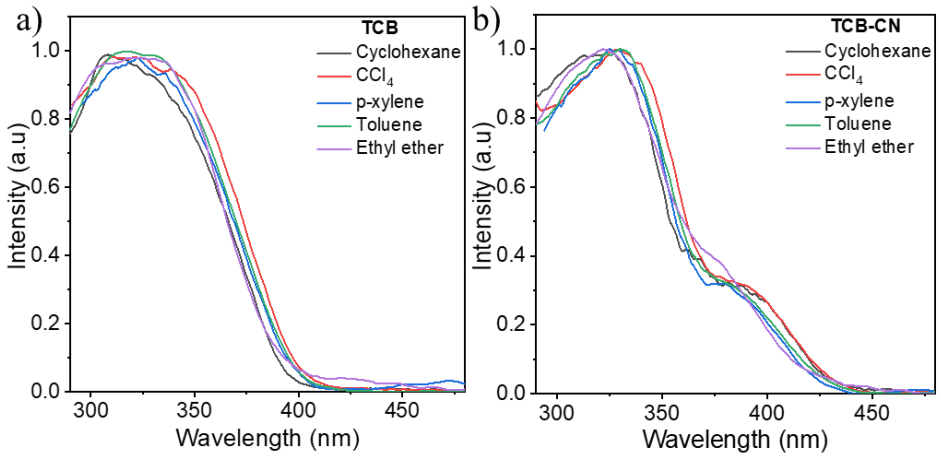

Fig.S1 UV-vis absorption spectrum of **TCB** and **TCB-CN** in various solvents (2×10^{-5}M)

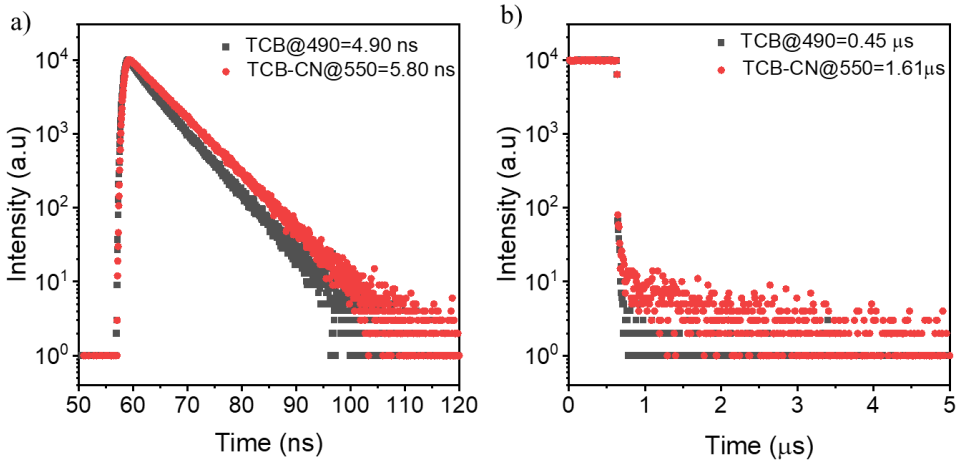

Fig.S2 Time-resolved decay curves of **TCB** and **TCB-CN** in toluene solution (2×10^{-5}M) at RT under air.

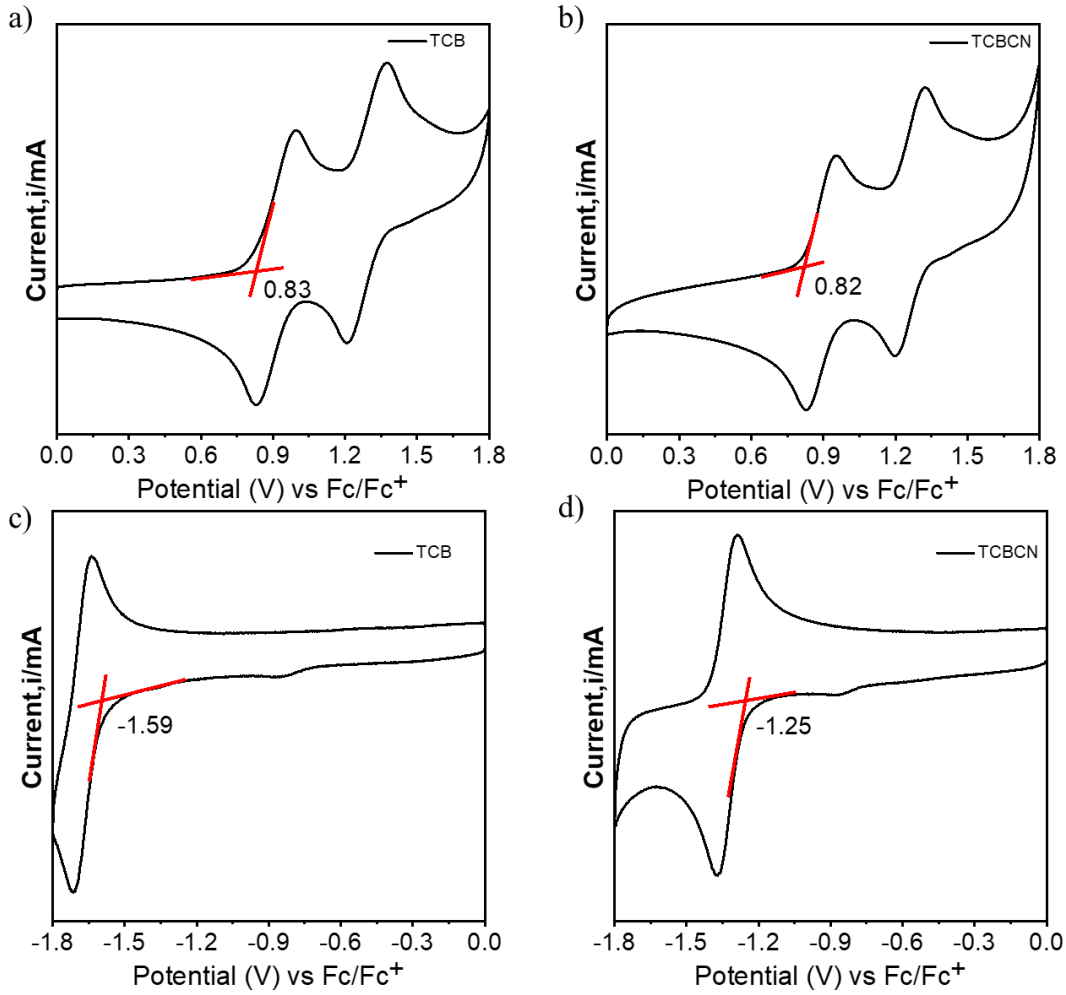

Fig.S3 Cyclic voltammograms of **TCB** and **TCB-CN**

The HOMO level was calculated from the oxidation half-wave potential with respect to $Fc|Fc^+$ redox couple using the following equation. The corresponding value for the LUMO level was estimated from the reduction onset potential using the following equation.

$$E_{HOMO} = - (E^{OX}_{1/2} \text{ (vs. } Fc^+/Fc)+4.8)$$
$$E_{LUMO} = - (E^{red}_{1/2} \text{ (vs. } Fc^+/Fc)+4.8)$$

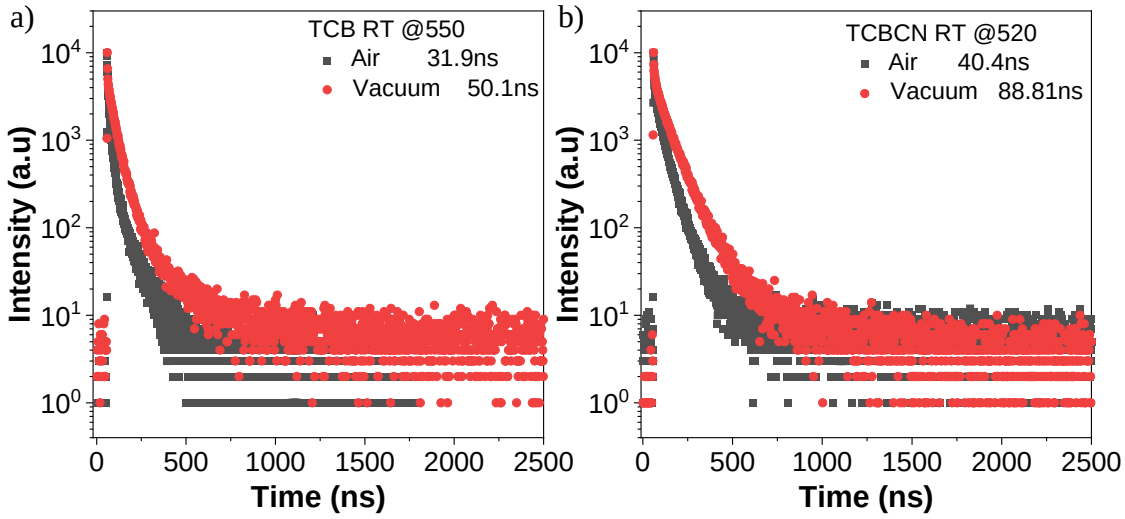

Fig.S4 Time-resolved decay curves of **TCB** and **TCB-CN** solid at RT under air and vacuo

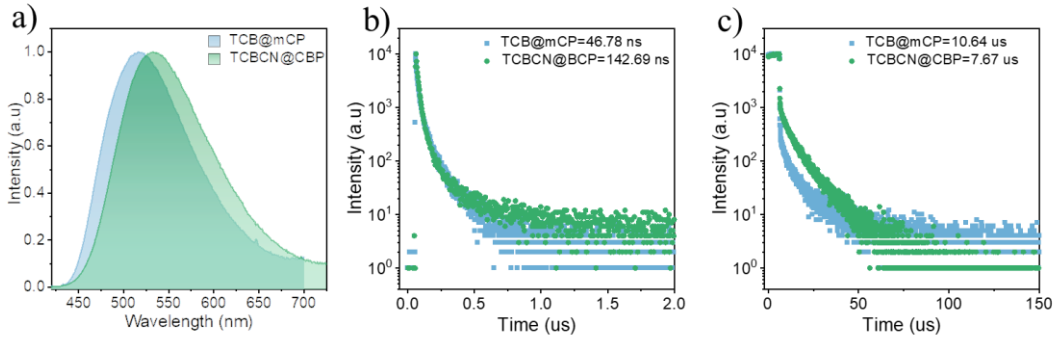

Fig.S5 (a)The steady-state emission spectrum of **TCB**-based and **TCB-CN**-based devices (b)-(c) Time-resolved decay curves of **TCB**-based and **TCB-CN**-based devices

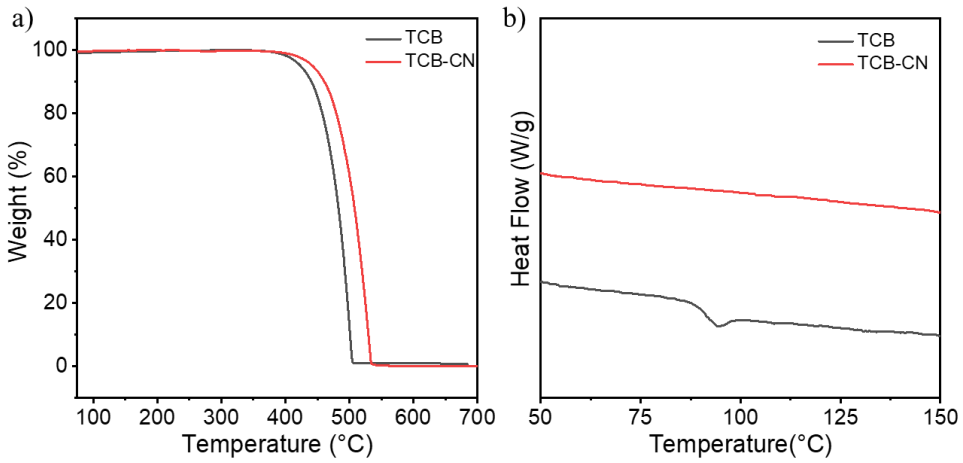

Fig.S6 TGA analysis and DSC analysis of **TCB** and **TCB-CN**

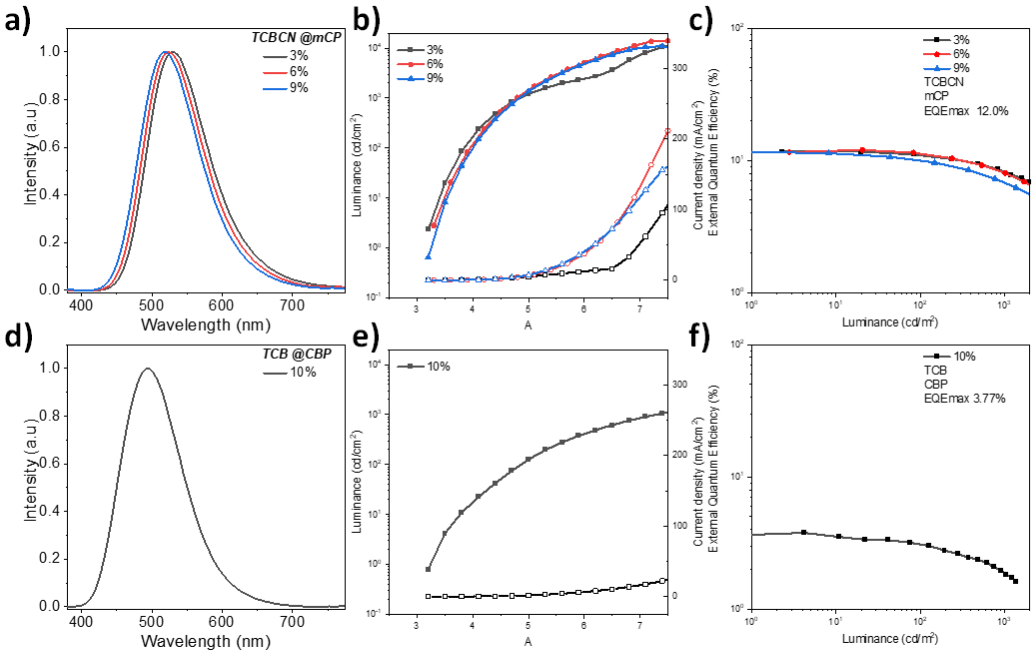

Fig.S7 The electroluminescence spectra of OLED devices recorded at 1000 cd/m^2 for **TCB-CN** (a) and **TCB** (d). The current density-voltage-brightness characteristics of OLED devices for **TCB-CN** (b) and **TCB** (e). The relationship between EQE-brightness and power efficiency-brightness of OLED devices fabricated from **TCB-CN** (c) and **TCB** (f).

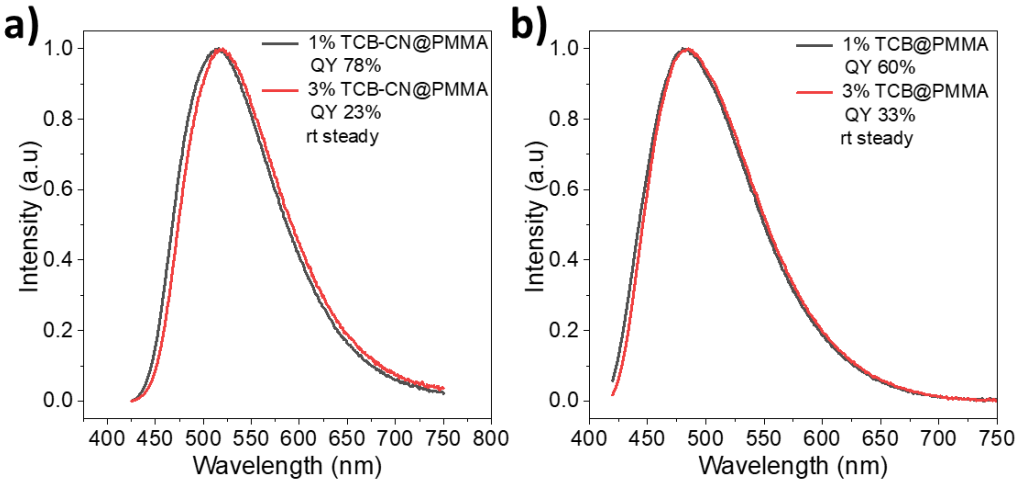

Fig.S8 Emission spectra of **TCB-CN** and **TCB** dopping in PMMA Films respectively at 298K.

Table S1. Summary of the performance of **TCB**-doped and **TCB-CN**-doped devices with different concentrations

Compounds	Doping ratio(%)	λ_{EL}/nm	V_{on}/V	CE_{max}/cd A^{-1}	PE_{max}/lm W^{-1}	EQE_{max}/%
TCB	5	488	3.8	11.0	9.0	4.5
	10	508	3.5	25.5	25.0	9.7
	15	512	3.4	28.1	28.4	10.3
	18	508	3.8	20.8	20.4	7.6
TCBCN	3	532	3.2	35.7	32.0	11.4
	5	528	3.3	48.4	46.1	15.6
	7	524	3.2	40.7	36.5	13.3
	10	536	3.2	30.2	29.6	9.7

a Doping concentration in mCP. b Turn-on voltage defined at 10 cd/m^2. c CE: current efficiency, PE: power efficiency, EQE: external quantum efficiency.

Table S2. Structure data of single crystals of **TCB, TCB-CN**.

Identification code	**TCB**	**TCB-CN**
Empirical formula	$C_{43}H_{30}N_2O$	$C_{45}H_{31}Cl_2N_3O$ (including CH_2Cl_2)
CCDC	No. 2106875	No. 2106876
Formula weight	590.69	700.63
Temperature/K	291(2)	291(2)
Crystal system	triclinic	triclinic
Space group	P-1	P-1
a/Å	9.2621(2)	10.6466(4)
b/Å	9.4236(3)	12.5874(5)
c/Å	18.3097(5)	14.0045(5)
α/°	79.048(2)	89.721(3)
β/°	84.422(2)	81.936(3)
γ/°	85.150(2)	72.136(3)
Volume/Å^3	1558.00(8)	1767.20(11)
Z	2	2
ρ_{calc}g/cm^3	1.259	1.317
μ/mm^{-1}	0.582	1.966
F(000)	620.0	728.0
Crystal size/mm^3	0.25 × 0.23 × 0.2	0.22 × 0.2 × 0.19
Radiation	CuK_α (λ = 1.54184)	CuK_α (λ = 1.54184)
2Θ range for data collection/°	9.582 to 140.008	7.384 to 139.988
Index ranges	-11 ≤ h ≤ 9, -11 ≤ k ≤ 11, -22 ≤ l ≤ 22	-10 ≤ h ≤ 12, -15 ≤ k ≤ 14, -14 ≤ l ≤ 17
Reflections collected	10276	12116
Independent reflections	5729 [R_{int} = 0.0174, R_{sigma} = 0.0258]	6520 [R_{int} = 0.0255, R_{sigma} = 0.0317]
Data/restraints/parameters	5729/0/416	6520/0/461
Goodness-of-fit on F^2	1.029	1.036
Final R indexes [I>=2σ (I)]	R_1 = 0.0389, wR_2 = 0.1029	R_1 = 0.0532, wR_2 = 0.1407
Final R indexes [all data]	R_1 = 0.0434, wR_2 = 0.1071	R_1 = 0.0652, wR_2 = 0.1519
Largest diff. peak/hole / e Å^{-3}	0.19/-0.16	0.67/-0.64

Table S3. Data extracted from the transient characterization of 5±1 wt% **TCB-CN**:CBP film and 15±1 wt% **TCB**:mCP film.

Compounds	Φ_{total}	Φ_F	Φ_{TADF}	k_P (s^{-1})	k_F (s^{-1})	k_{ISC} (s^{-1})	k_{TADF} (s^{-1})	k_{RISC} (s^{-1})	k_{nr}^T (s^{-1})
TCB	42	17.64	24.36	$2.14*10^7$	$3.77*10^6$	$1.76*10^7$	$6.63*10^4$	$1.15*10^5$	$4.60*10^4$
TCB-CN	63	20.16	42.84	$7.01*10^6$	$1.41*10^6$	$5.58*10^6$	$1.11*10^5$	$2.95*10^5$	$5.17*10^4$

$$k_P = \frac{1}{\tau_p}$$

$$k_F = k_p \Phi_F$$

$$k_F = k_p + k_{ISC}$$

$$k_{TADF} = \frac{\Phi_{TADF}}{\Phi_{ISC} \tau_{TADF}}$$

$$k_{RISC} = \frac{k_p k_{TADF}}{k_{ISC}} \frac{\Phi_{TADF}}{\Phi_F}$$

$$k_{nr}^T = k_{TADF} - \left(1 - \frac{k_{ISC}}{k_F + k_{ISC}}\right) k_{RISC}$$

where Φ_F is the fluorescence quantum efficiency and Φ_{TADF} is the delayed fluorescence quantum efficiency, Φ_F and Φ_{TADF} are estimated from the Φ_{total} with a relative ratio which was calculated from the transient PL spectra according to the literature.[1-2] Φ_{ISC} is the ISC efficiency; k_P, k_F, k_{ISC} k_{TADF} and k_{RISC} are the rate constants of prompt fluorescence, fluorescence decay, the ISC, delayed fluorescence decay and the RISC respectively; k_{nr}^T is the nonradiative decay rate constant of triplet excitons.

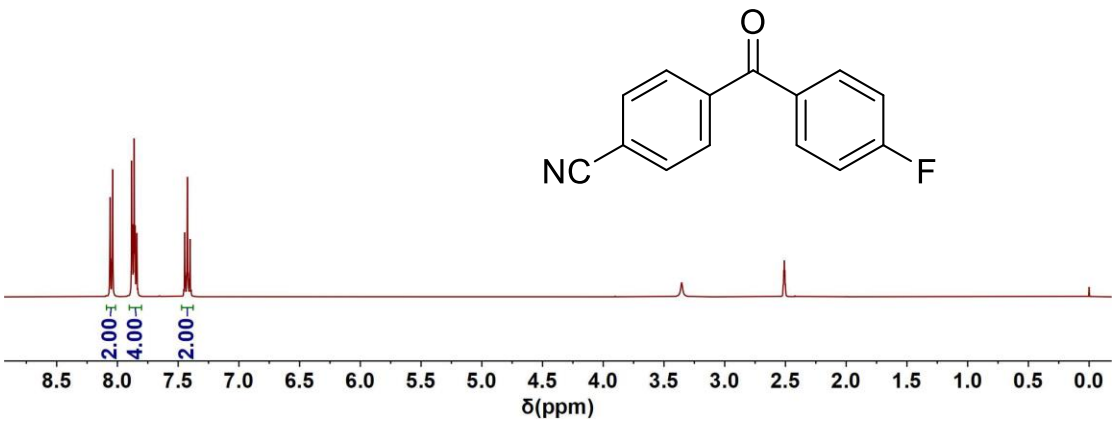

Fig.S9 ^{1}H NMR spectrum of **B-CN** in DMSO.

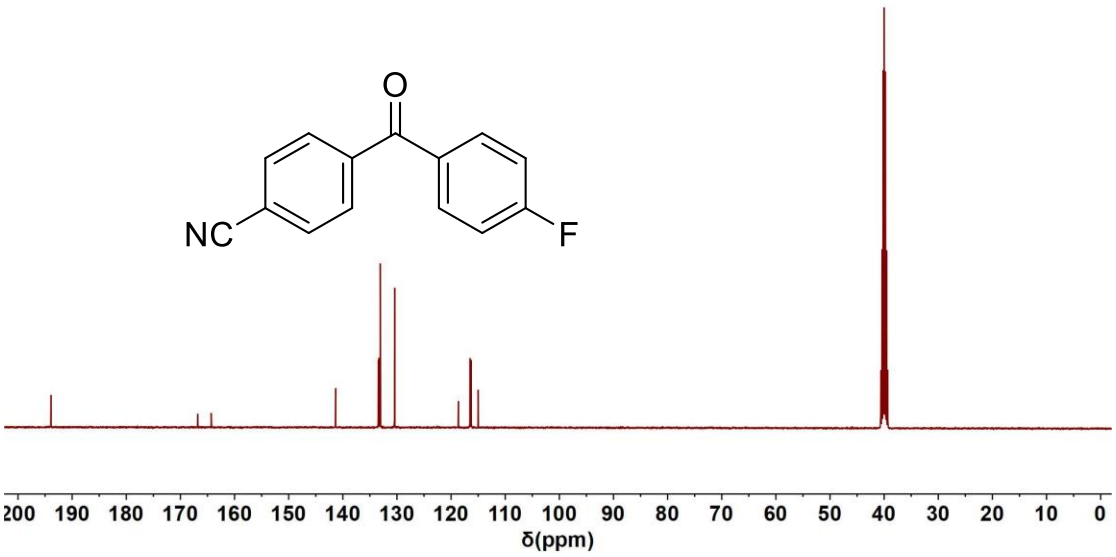

Fig.S10 ^{13}C NMR spectrum of **B-CN** in DMSO.

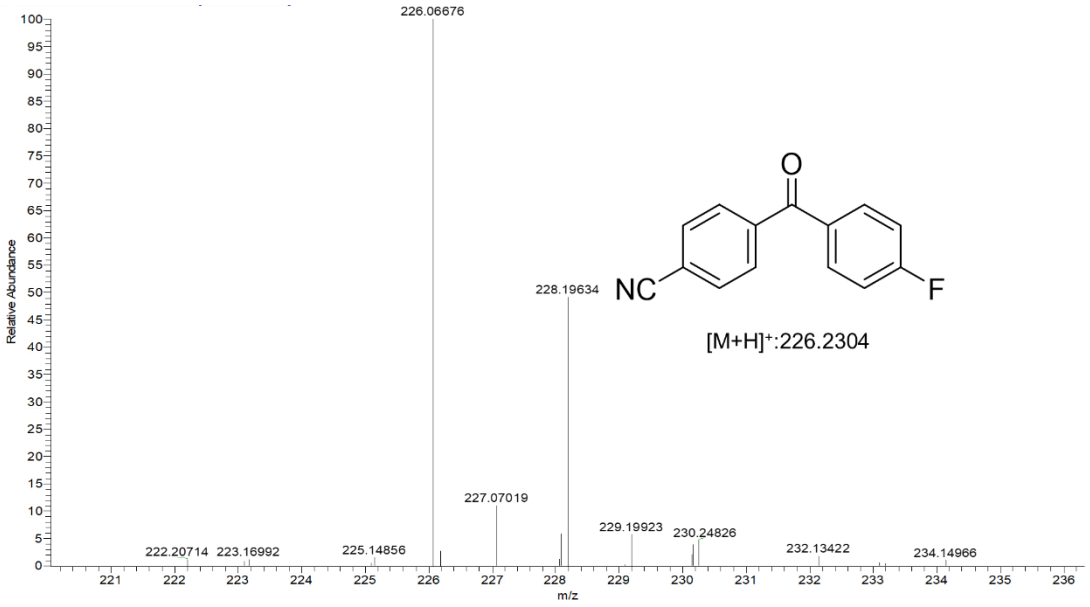

Fig.S11 ESI mass spectrum of **B-CN**.

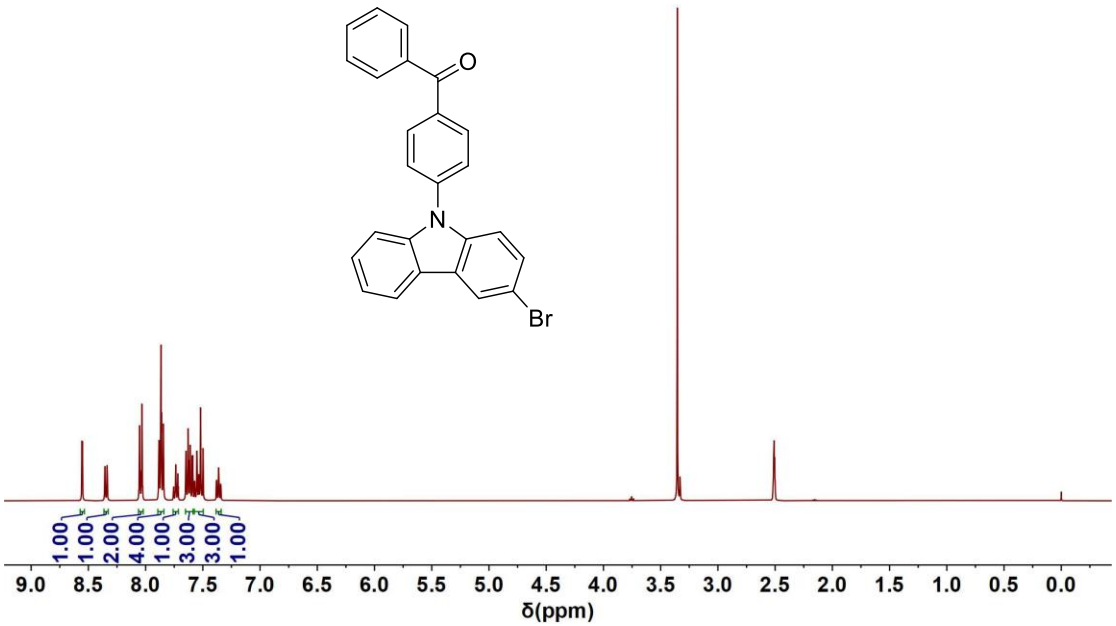

Fig.S12 ^{1}H NMR spectrum of **CB** in DMSO.

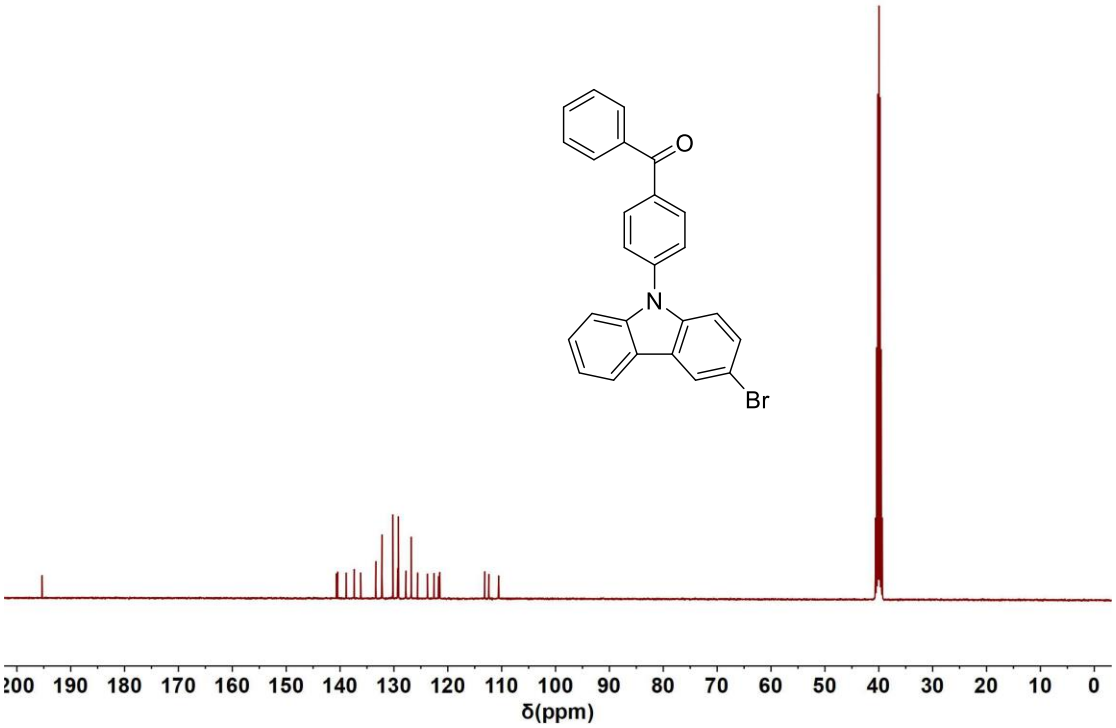

Fig.S13 ^{13}C NMR spectrum of **CB** in DMSO.

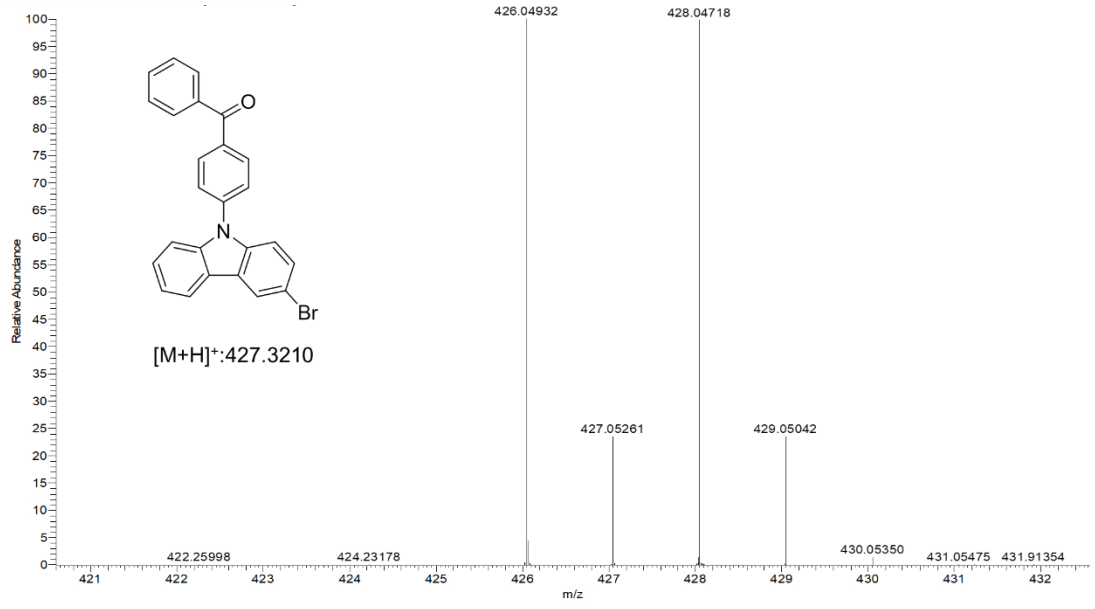

Fig.S14 ESI mass spectrum of **CB**.

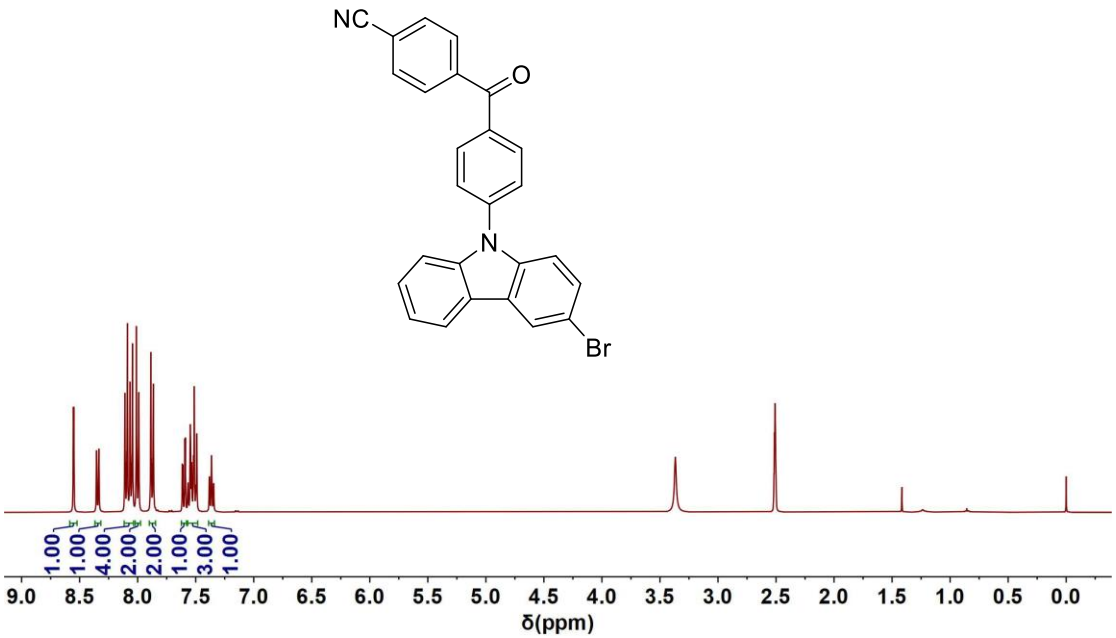

Fig.S15 ^{1}H NMR spectrum of **CB-CN** in DMSO.

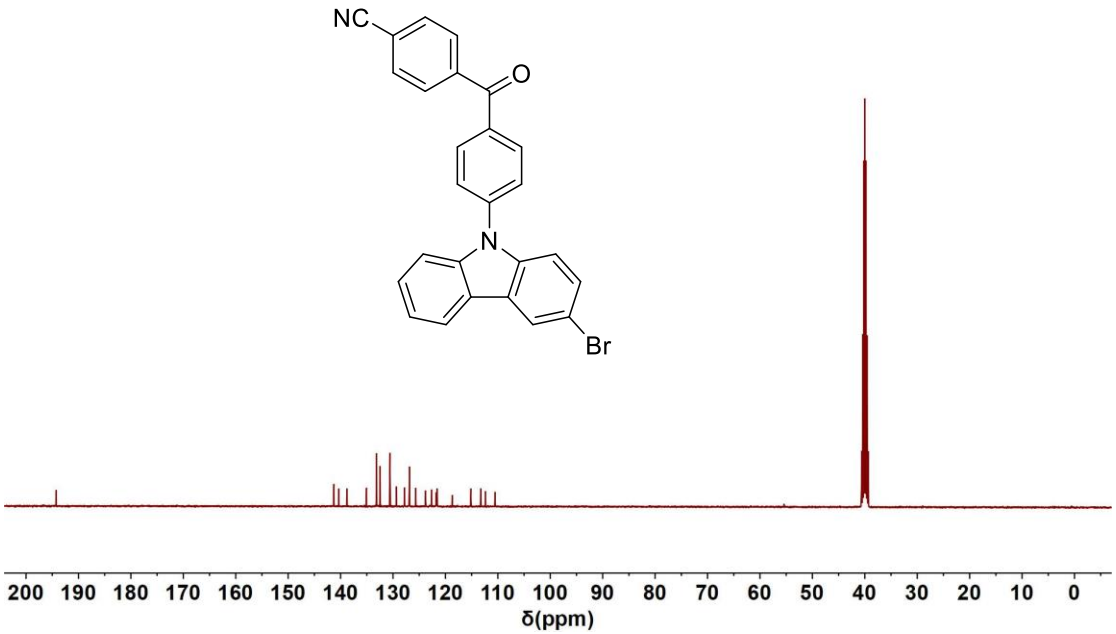

Fig.S16 ^{13}C NMR spectrum of **CB-CN** in DMSO.

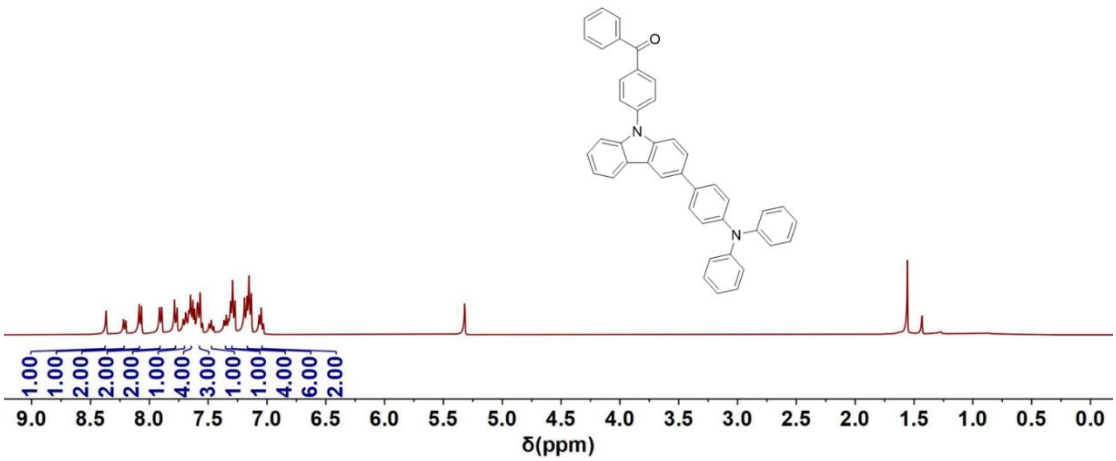

Fig.S17 ^{1}H NMR spectrum of **TCB** in CD_2Cl_2.

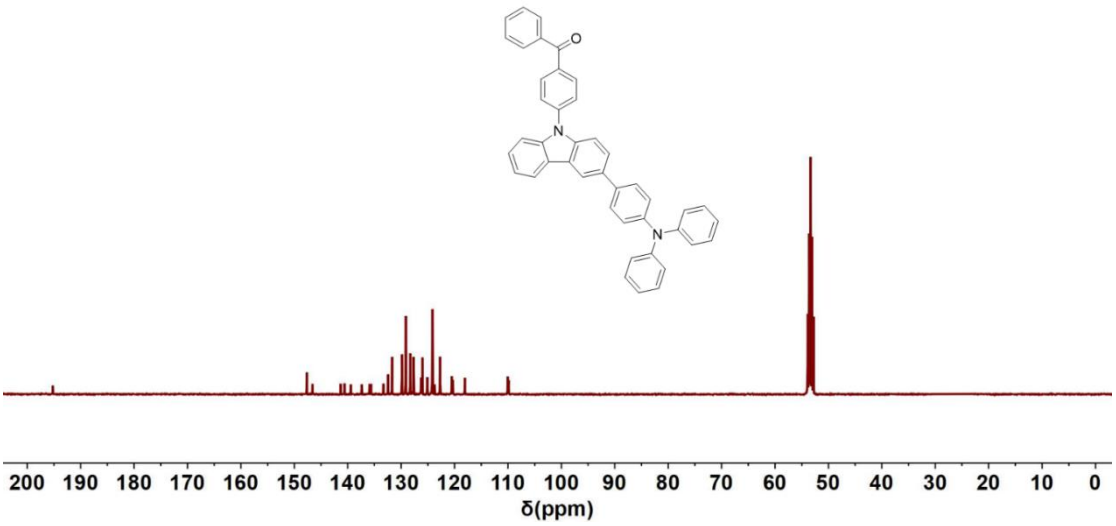

Fig.S18 ^{13}C NMR spectrum of **TCB** in CD_2Cl_2.

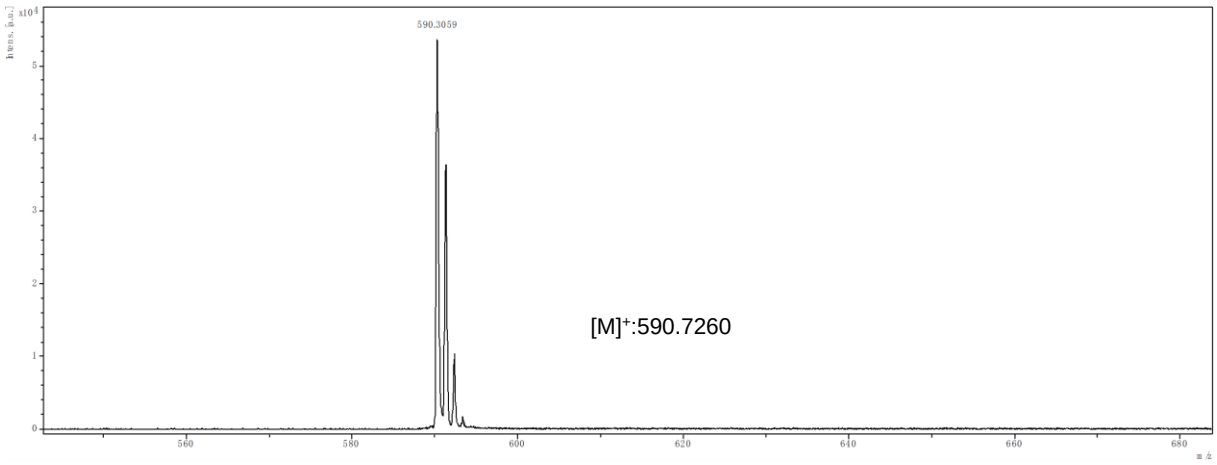

Fig.S19 MALDI-TOF mass spectrum of **TCB**.

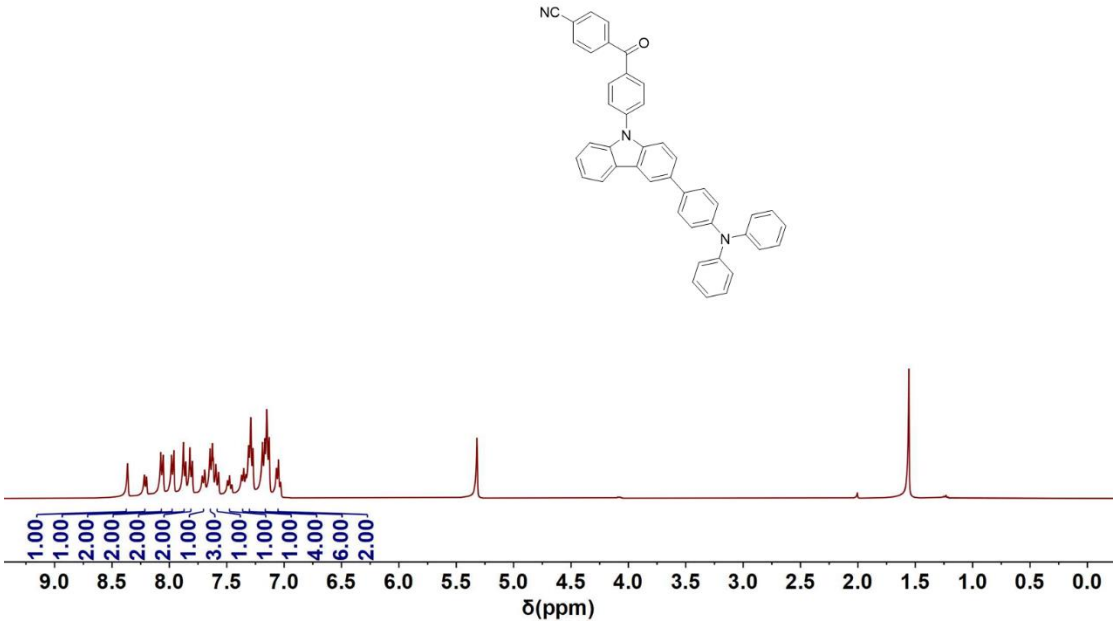

Fig.S20 ^{1}H NMR spectrum of **TCB-CN** in CD_2Cl_2.

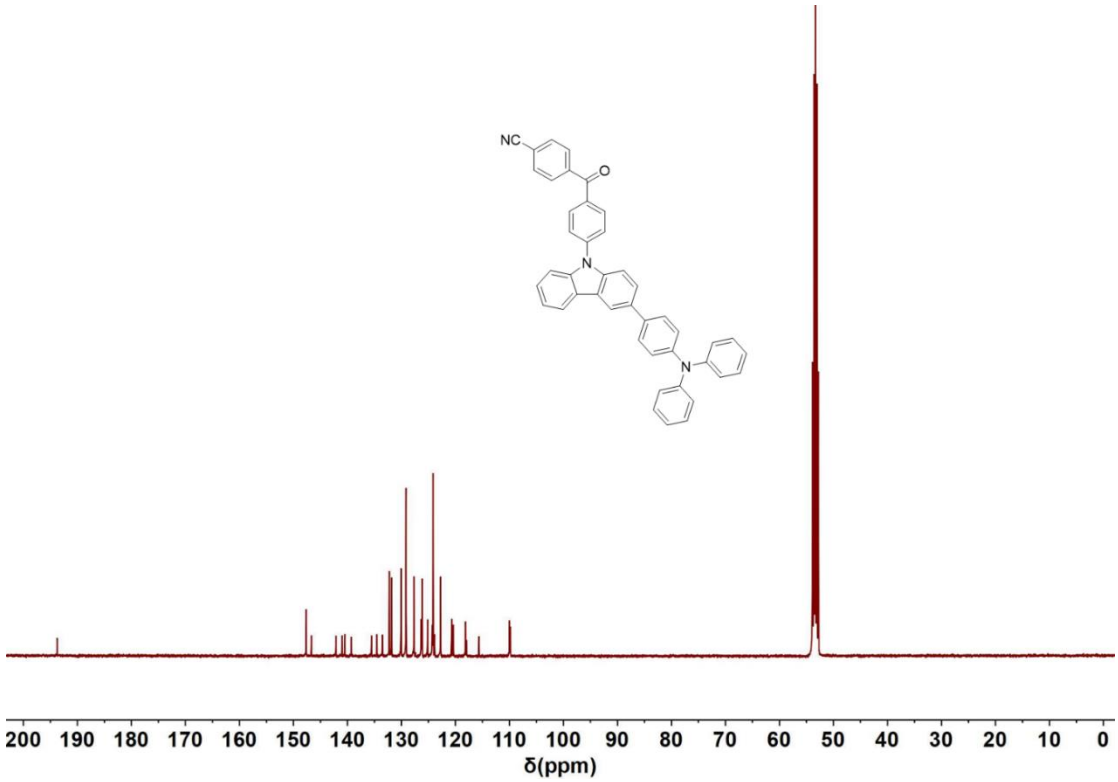

Fig.S21 ^{13}C NMR spectrum of **TCB-CN** in CD_2Cl_2.

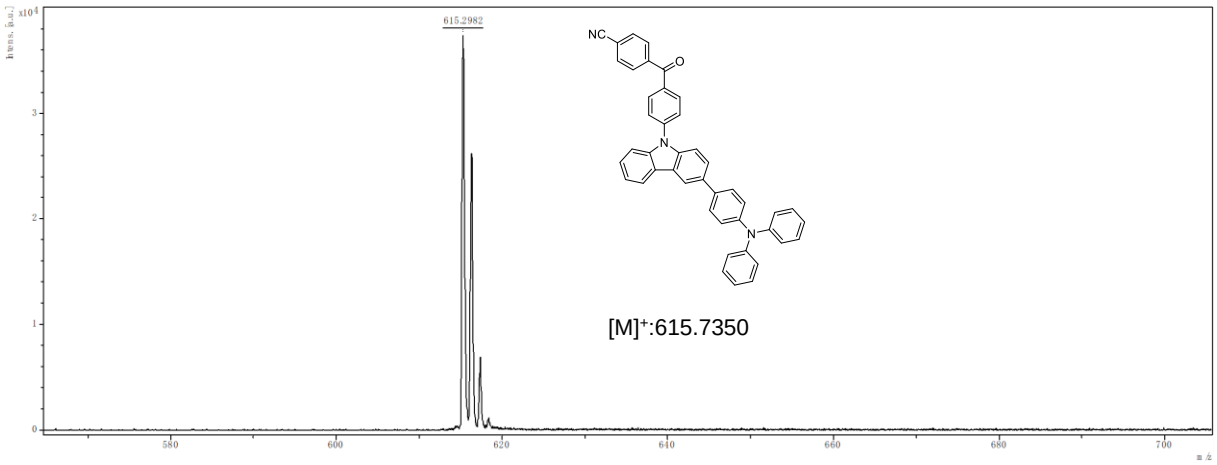

Fig.S22 MALDI-TOF mass spectrum of **TCB-CN**.

References

1 H. Wang, L. Xie, Q. Peng, L. Meng, Y. Wang, Y. Yi, P. Wang, *Adv. Mater.* 2012, **26**, 5198;

2 J.X. Chen, K. Wang, C.J. Zheng, M. Zhang, Y.Z. Shi, S.L. Tao, H. Lin, W. Liu, W.W. Tao, X.M. Ou, X.H. Zhang, *Adv Sci*. 2018,**5**,1800436.